Journal of Volcanology and Geothermal Research 289 (2014) 193–201

Contents lists available at ScienceDirect

Journal of Volcanology and Geothermal Research

journal homepage: www.elsevier.com/locate/jvolgeores

Crustal imaging of western Michoacán and the Jalisco Block, Mexico, from Ambient Seismic Noise

Zack Spica *, Víctor M. Cruz-Atienza, Gabriel Reyes-Alfaro, Denis Legrand, Arturo Iglesias-Mendoza

Instituto de Geofísica, Universidad Nacional Autónoma de México, Mexico

ARTICLE INFO

Article history:
Received 6 June 2014
Accepted 12 November 2014
Available online 20 November 2014

Keywords:
Tomography
Ambient noise
Colima volcano
Magma reservoirs
Rivera-Cocos plates

ABSTRACT

Detailed crustal imaging of western Michoacán and the Jalisco Block is obtained from ambient noise tomography. Results show a deep and well-delineated volcanic system below the Colima volcano complex, rooting up to ~22 km depth, with a shallow magmatic chamber constrained to the first ~7 km. A shallow low-velocity system to the south of the Chapala rift and west of the Michoacán-Guanajuato volcanic field merges, underneath the Colima rift, with the Colima volcano system at about 20 km depth, honoring the geometry of the Trans-Mexican Volcanic Belt. For depths greater than ~30 km, low-velocity features become parallel to the slab strike, right beneath the Mascota, Ayutla and Tapalpa volcanic fields, suggesting the presence of the mantle wedge above the Rivera plate. All mentioned low-velocity bodies are spatially correlated with the superficial volcanic activity suggesting their magmatic origin so that, the shallower these bodies, the younger are the associated volcanic deposits. Along the coast, different depths of the uppermost layer of the Rivera and the Cocos plates suggest that the latter plate subducts with an angle ~9° steeper than the former.

1. Introduction

In western Mexico, the Rivera and the Cocos oceanic plates subduct beneath the North American continental plate (Fig. 1). Both oceanic plates have different ages, compositions (e.g., Schaaf et al., 1995; Rosas-Elguera et al., 1996), convergence vectors and subduction angles (Kostoglodov and Bandy, 1995; Pardo and Suárez, 1995; Manea et al., 2006; Pérez-Campos et al., 2008; Soto et al., 2009; Yang et al., 2009; Andrews et al., 2011; Skinner and Clayton, 2011; Suhardja, 2013; Taran et al., 2013; Abbott, 2014). Five to 10 Ma ago, the Rivera plate that subducts the Jalisco Block detached from the Cocos plate (DeMets and Traylen, 2000), generating an extensional rifting process that separates the Jalisco Block from the North American plate (e.g., Bandy et al., 2000; Ferrari and Rosas-Elguera, 2000). Although the Jalisco Block is well delineated by the Colima graben to the East and the Tepic-Zacoalco rift to the North (Fig. 1), the nature and the exact location of the boundary between both subducting plates are still unclear (e.g., Andrews et al., 2011; Gaviria et al., 2013). At present, it is believed that the boundary lies beneath the Colima graben on land and the El Gordo graben offshore (e.g., Serrato-Díaz et al., 2004; Dougherty et al., 2012), but the existing uncertainty makes it challenging to understand the dynamic interaction between the Rivera plate and the deformation of the overriding Jalisco Block.

The rifting structures bounding the Jalisco Block along with the subduction process have produced spatio-temporal variations of the volcanism in the Jalisco Block and the western part of the Trans-Mexican Volcanic Belt (TMVB). Geochemical analysis of lava sampled in the region revealed contrasting compositions, including both subduction-related calk-alkaline and intraplate alkaline volcanic signatures (e.g., Ferrari et al., 2000). Furthermore, the volcanic front in the western TMVB has migrated trenchward from the late Miocene to the Quaternary (Ferrari et al., 2001). This migration may be related to the steepening of the Rivera plate, due to a reduction of its convergence rate about 8.5 to 6.5 Ma ago (e.g., Pardo and Suárez, 1995) (i.e., a slab rollback; Ferrari et al. (2001)). Although Frey et al. (2007) are skeptical of the trenchward slab migration due to a lack of geological evidence, recent seismological studies support the "rollback theory", which seems to explain a lateral asthenospheric flow around the slab edges toward the mantle wedge (Soto et al., 2009; Yang et al., 2009; Suhardja, 2013; Ferrari et al., 2011). Furthermore, shear-waves splitting and P-wave tomographic studies (Soto et al., 2009; Yang et al., 2009) support the idea of a slab gap between the Rivera and the Cocos plates (deeper than 150 km) starting just north of the Colima volcano. This aperture would also allow deep and enriched asthenospheric materials to flow into the mantle wedge. Furthermore, Yang et al. (2009) proposed the existence of a slab detachment in the Rivera plate (about 400 km depth) that allows material to rise and produce a locally warmer mantle wedge. These recent results (Yang et al., 2009) may explain the mixed geochemical signature of the western TMVB basalts.

The 'Mapping the Rivera Subduction Zone' (MARS) and the 'Colima Volcano Deep Seismic Experiment' (CODEX) seismic arrays (Fig. 1) have significantly contributed to the understanding of the deep structure (i.e., below 80 km depth) and geodynamics of the region. Some

* Corresponding author.
E-mail address: zackspica@geofisica.unam.mx (Z. Spica).

http://dx.doi.org/10.1016/j.jvolgeores.2014.11.005
0377-0273/

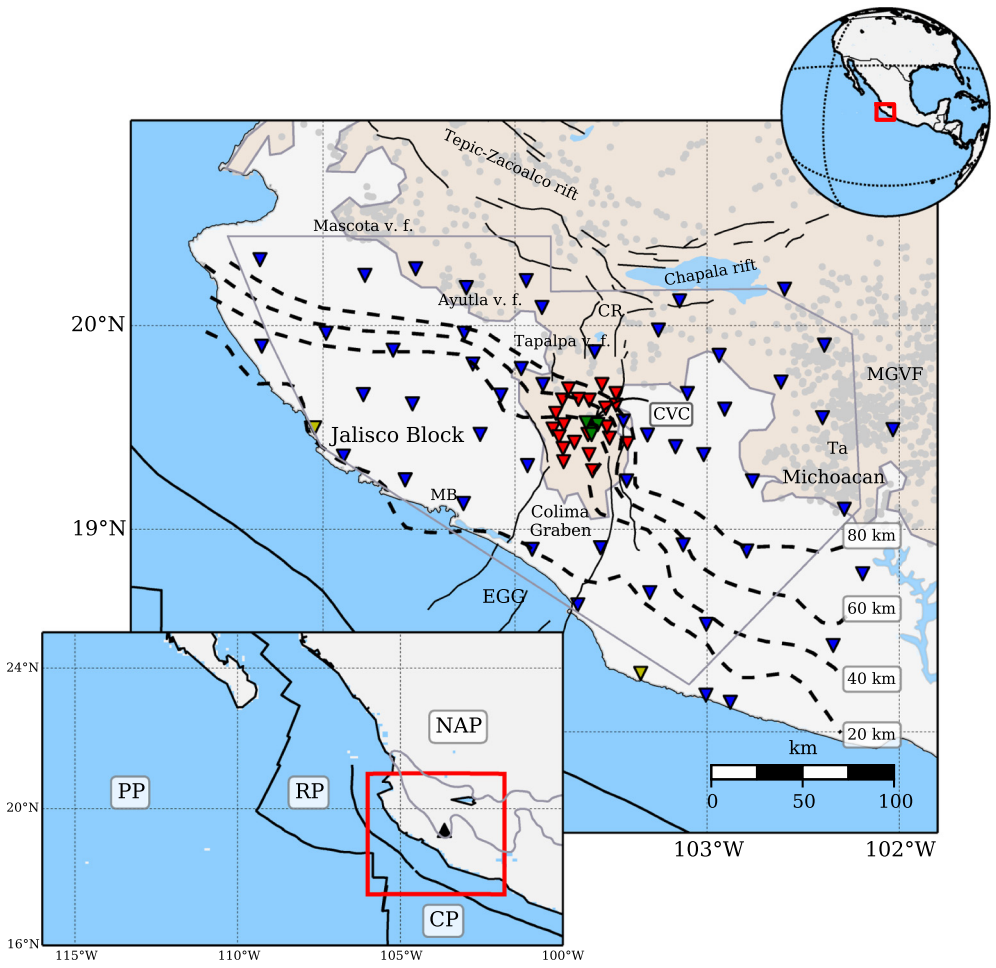

Fig. 1. Tectonic and geologic setting of the study region. Triangles correspond to the seismic stations: MARS (blue); CODEX (red); RESCO (green); SSN (yellow). The study region is delineated by the grey polygon. Gray dots refer to the monogenetic volcanoes (from Ferrari et al., 2011). The acronyms are as follows: CP, coco plate; CR, Colima rift; CVC, Colima volcanic complex; EGG, El Gordo graben; MB, Manzanillo Bay; MGVF, Michoacan-Guanajuato volcanic field; NAP, North American Plate; PP, Pacific plate; RP, Rivera plate; Ta, Tancítaro stratovolcano. Tectonic features (black lines), the Trans-Mexican Volcanic Belt (sandy colored region) and slab isodepth contours (black dotted lines) are taken from Yang et al. (2009), Ferrari et al. (2011) and Abbott (2014), respectively.

authors (Andrews et al., 2011; Taran et al., 2013; Abbott, 2014) suggest that a sharp change in the slab subduction angle takes place beyond 40 km inland from the coast at ~35 km depth, so that the Rivera plate becomes steeper than the Cocos plate (dotted lines in Fig. 1). Despite these works, the continental crust is still poorly known. The absence of information responds to the limitations of traditional tomographic techniques based on passive seismology (i.e., earthquake records), which often lack of resolution in the shallow structure due to inadequate ray coverage in the crust. A better understanding of the relationship between the deep geodynamic processes and both seismotectonics and superficial geology (e.g., the active volcanism) requires a detailed description of the crust. To do so, we performed an ambient noise surface wave tomography, which is a technique allowing producing high-resolution images of the upper crust in the absence of earthquakes (e.g., Shapiro et al., 2005; Brenguier et al., 2007; Stehly et al., 2009; Stankiewicz et al., 2010; Mordret et al., 2013). The technique retrieves the elastodynamic Green's function (EGF) between pairs of stations in a large frequency range (depending of the seismic network configuration) by cross-correlating the ambient noise time series recorded at the stations (Shapiro and Campillo, 2004; Shapiro et al., 2005; Weaver, 2005; Shen et al., 2012).

In this work, we first explain (Section 3) the methodology used to recover the EGFs between concomitant pairs of stations of four seismic networks: (1) the Mapping the Rivera Subduction Zone (MARS) experiment, (2) the Colima Volcano Deep Seismic Experiment (CODEX); (3) the Colima local network (RESCO); and (4) the National Seismological Service (SSN) network. Then we describe how the Rayleigh-wave group velocity measurements were generated from these EGFs (also in Section 3) to carry out the crustal tomographic imaging (Section 4). We finally analyze and interpret the obtained images (Section 5) of the upper 35 km across the Jalisco Block and western Michoacán, under the light of previous studies.

2. Seismic data processing

The spatial resolution of ambient noise tomography depends on the frequency bandwidth of the seismic measurements and both the density and distribution of the stations. Seismic networks with small interstation spacing, large footprints and long deployment duration are appropriate for detailed ambient noise studies (Sánchez-Sesma and Campillo, 2006; Bensen et al., 2007). In this work, we compiled seismic data from four different networks (Fig. 1; MARS, CODEX, RESCO and SSN) that continuously recorded the ground motion. The temporal MARS experiment (Yang et al., 2009) consisted of 50 broadband seismic instruments deployed in southwestern Mexico during 18 months from January 2006 to June 2007. The CODEX experiment, which had a five-month overlap with the MARS experiment, consists of 18 short-period seismic instruments deployed in the surroundings of the Colima Volcano. The RESCO and the SSN permanent networks, have broadband seismometer from which we used continuous records between January 2006 and

March 2008. In total, 78 seismic stations were used to obtain vertical component cross-correlation functions (CCFs) for daily time series of all concomitant pairs of stations. We pre-processed the data by down sampling to 20 Hz, removing of the mean, the trend and the instrumental response, followed by a 1- to 40-s band-pass filtering. Temporal (1 bit) and spectral (whitening) normalizations were also applied to diminish the influence of earthquakes and non-stationary noise sources near the stations, but also to broaden the observed frequency band (e.g., Bensen et al., 2007). The daily CCFs were stacked for each station pair to improve the signal-to-noise ratio (SNR). Only CCFs with SNR larger or equal to 15 were used in the study. Forty-six percent of the obtained CCFs were rejected after applying such quality criterion. Fig. 2 shows the resulting CCFs as a function of interstation distance, where a coherent wave train propagating across the network is clearly observed. To retrieve the EGF between pairs of seismometers, the CCFs were finally folded at the origin time and stacked to further enhance the SNR and to reduce the effect of sources distribution (e.g., Sabra et al., 2005). Since we only considered the vertical component of ground motions, our EGFs are dominated by Rayleigh waves.

From the EGFs, we extracted the surface wave group velocities by means of a frequency time analysis (FTAN; e.g., Dziewonski et al., 1969). The FTAN technique applies a set of Gaussian filters with different dominant frequencies to the input-signal spectrum. The arrival times for each frequency band are then estimated from the maxima of the time envelopes (i.e., group velocities). However, the FTAN method leads to systematic errors in the group velocity estimates due to variations in the spectral amplitudes that shift the central frequency toward the origin of the filtered spectrum (Levshin, 1989). This shift was corrected by considering the centroid frequency (Shapiro and Singh, 1999), which is the frequency where the filtered spectrum reaches its maximum. The resulting dispersion curves were visually selected. Only the group travel times for stations separated by more than three wavelengths were accepted (Bensen et al., 2007). Besides, curves with incoherent dispersion patterns were also rejected (i.e., the group velocity do not vary smoothly with the period) using as a reference the average dispersion curve obtained for the region by Iglesias et al. (2001). Examples of dispersion curves between the EFRE station at the center of the study region (RESCO network) and many others with a complete azimuthal coverage are shown in Fig. 3A and B. Fig. 3C also shows an example of FTAN diagram obtained for the station pair EFRE-MA11 (RESCO-MARS; thicker blue lines in Fig. 3A and B).

3. Group velocity tomography

We obtained Rayleigh-wave group velocity maps from the picked travel times at different periods (i.e., 3, 5, 10, 15, 20 and 25 s) by means of a non-linear iterative 2-D tomographic technique (Rawlinson et al., 2008; Saygin and Kennett, 2010). At each iteration, the ray paths between stations were updated so that the influence of their length is taken into account to compute theoretical arrival times. This step was carried out by the fast marching method (FMM) (Sethian, 1996; Rawlinson and Sambridge, 2004). The FMM is a grid-based Eikonal

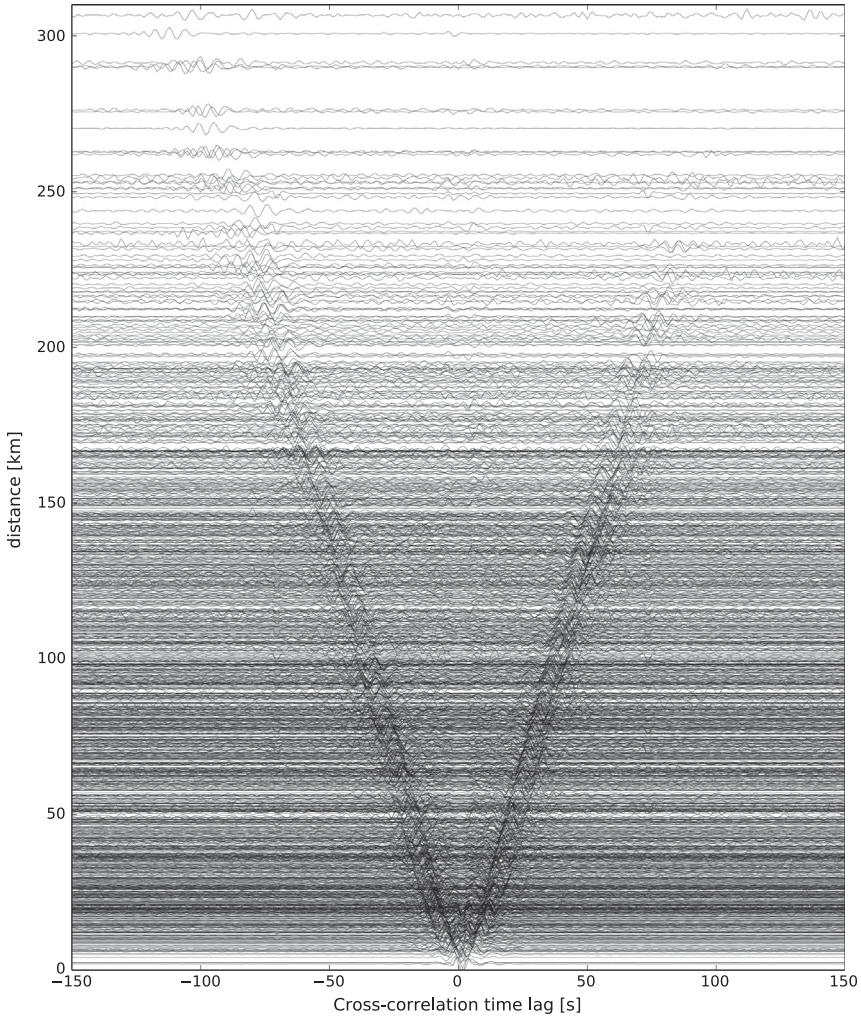

Fig. 2. Band-pass filtered (10 s) EGFs with SNR higher than 15 as a function of interstation distance.

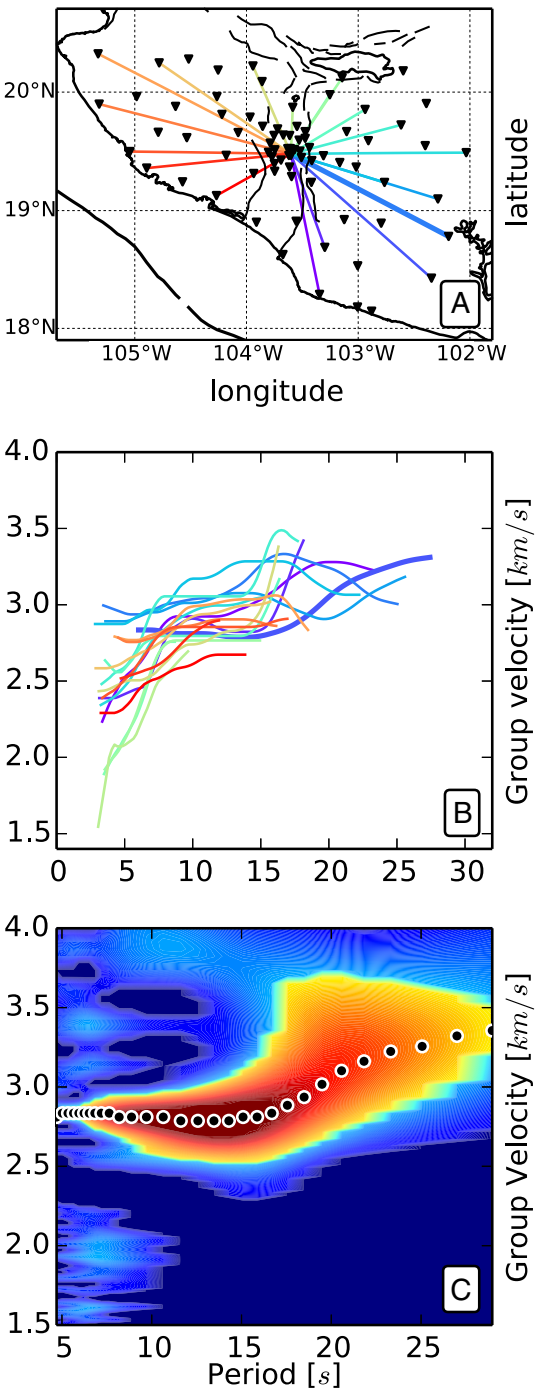

Fig. 3. Examples of Rayleigh-wave dispersion curves. (A) Ray paths over a complete azimuthal range with dispersion curves (color coded) shown in panel B. (B) Dispersion curves for propagation paths shown in panel A. (C) FTAN spectrum (dispersion diagram) for the station pair EFRE-MA11 (thick blue lines in panels A and B).

solver that uses implicit wavefront construction and provides stable and robust solutions for wave propagation in highly heterogeneous media (Rawlinson and Sambridge, 2004; de Kool et al., 2006). The inversion method then seeks for the perturbation of the model parameters that better match the group velocity measurements. Once the perturbations are estimated, the model is updated and propagation paths are retraced using the FMM scheme. In this study, we used the Fast Marching Surface Wave Tomography code developed by N. Rawlinson in the framework of the aforementioned studies.

For each period of interest, a set of 2D inversions (i.e., over horizontal planes) was performed from the associated group velocity measurements, using a regular grid with spatial increments of 0.18° × 0.16° in latitude and longitude, respectively. The inversions were carried out starting with homogeneous velocity models equal to the mean velocity of each set of group speeds observed for the selected period. Based on travel-time misfit values, we used standard L-curve analysis (e.g., Menke, 2012) to determine the optimum weights (in a range of value from 0 to 10,000) for the spatial smoothing and damping.

We performed synthetic checkerboard tests with the available path distribution at different periods to investigate the resolution of our tomographic images. We set an initial 2D problem composed of an alternating pattern of low and high velocity perturbations (i.e., square cells with 25 km per side; Fig. 4) and then try to recover the pattern with the available path coverage for different periods (Fig. 5) using the same inversion procedure. The synthetic inversion results are given in Fig. 4 and show that the overall recovery of the velocity pattern is good for periods smaller or equal to 20 s. At 25 s, resolution degrades due to a significant reduction of paths density (Fig. 5), but it is still possible to extract useful information. A smearing effect is observed in all periods close to the edges of the station ray so that results should be interpreted carefully in these regions. To exclude most of the unresolved zones of the model from our analysis, we defined a "satisfactory-resolution-box" (dashed polygon in Figs. 4, 5 and 6), where our results can be interpreted with fair enough confidence. The box excludes the offshore and east-southeast areas of the model, where the smearing of the checkerboards is evident for all periods.

Checkerboard tests can fail to recover certain kind of velocity anomalies. For example, Lévêque et al. (1993) demonstrated that, for certain path coverage, the tests recover much better small patterns than larger structures. Thus, care should be taken when evaluating the results yielded by this kind of synthetic inversions. An alternative strategy to estimate the resolution consists of analyzing the density of ray paths at different periods (Fig. 5). In our case, a maximum number of 1136 paths were obtained for the shortest period of 5 s. For longer periods, the number of paths gradually decreases down to a minimum value of 176 for the longest period of 25 s. The best-fitting Rayleigh-wave group velocities maps are shown in Fig. 6 along with their associated rms travel-time residuals.

4. Results and discussion

In order to assess the depth-range sampled in each tomographic map, we computed sensitivity kernels for the Rayleigh-wave fundamental mode (Herrmann, 1989) at the periods shown in Figs. 4, 5 and 6. Since our study area encompasses different geological settings, to compute the kernels we chose two distinct velocity structures obtained for the region: (1) a model determined beneath the Popocatépetl volcano (Cruz-Atienza et al., 2001), which includes both the superficial volcanic deposits associated to the TMVB and a low-velocity zone associated to the volcano magma chamber; and (2) a typical crustal model determined along the coast in southern Mexico (Iglesias et al., 2001) (middle panel, Fig. 7). The kernels (left panel, Fig. 7) reveal the sensitivity of the surface waves to small perturbations in depth for the model elastic properties (Aki and Richards, 2002). Their maxima indicate the depths where the corresponding eigenfunctions are primarily determined by the model. The right panel of Fig. 7 shows the depth ranges where sensitivity is higher than 85% of the maximum values. As expected, the longer the period of the surface waves, the larger is the range of depths with similar sensitivity. From now on, attributed depths in the discussion and conclusion sections are based on these estimates.

4.1. The Colima volcano complex

The most striking feature in Fig. 6 for all periods is a low-velocity zone below the Colima volcano (denoted as "a" in the 5 s map of Fig. 6). For

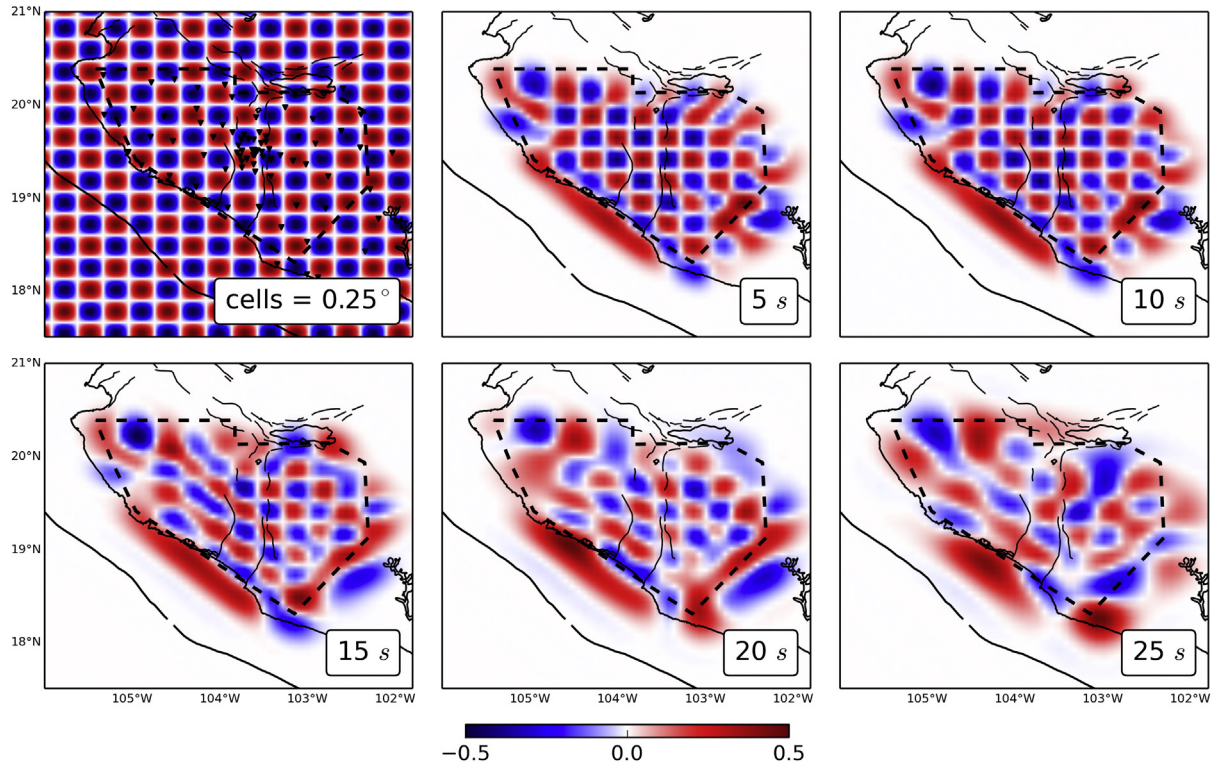

Fig. 4. Checkerboard tests for different periods. The upper-left panel shows the target checkerboard model (i.e., velocity perturbations; color scale). The other panels show the inversion results for 5-, 10-, 15-, 20- and 25-s period. Stations are depicted with black triangles. The black dashed polygon represents the satisfactory-resolution-box. Major tectonic features (black lines) are the same as in Fig. 1.

the 3- and 5-s period maps (i.e., above ~7 km depth), we find very low group velocities of ~1.6 km/s. Although no physical characterization can be directly inferred from our measurements, we naturally associate this zone to the presence of the shallow-crust magma body responsible of the current Colima volcano activity (e.g., Lees, 2007). Similar observations were obtained for group velocity maps at Yellowstone (Stachnik

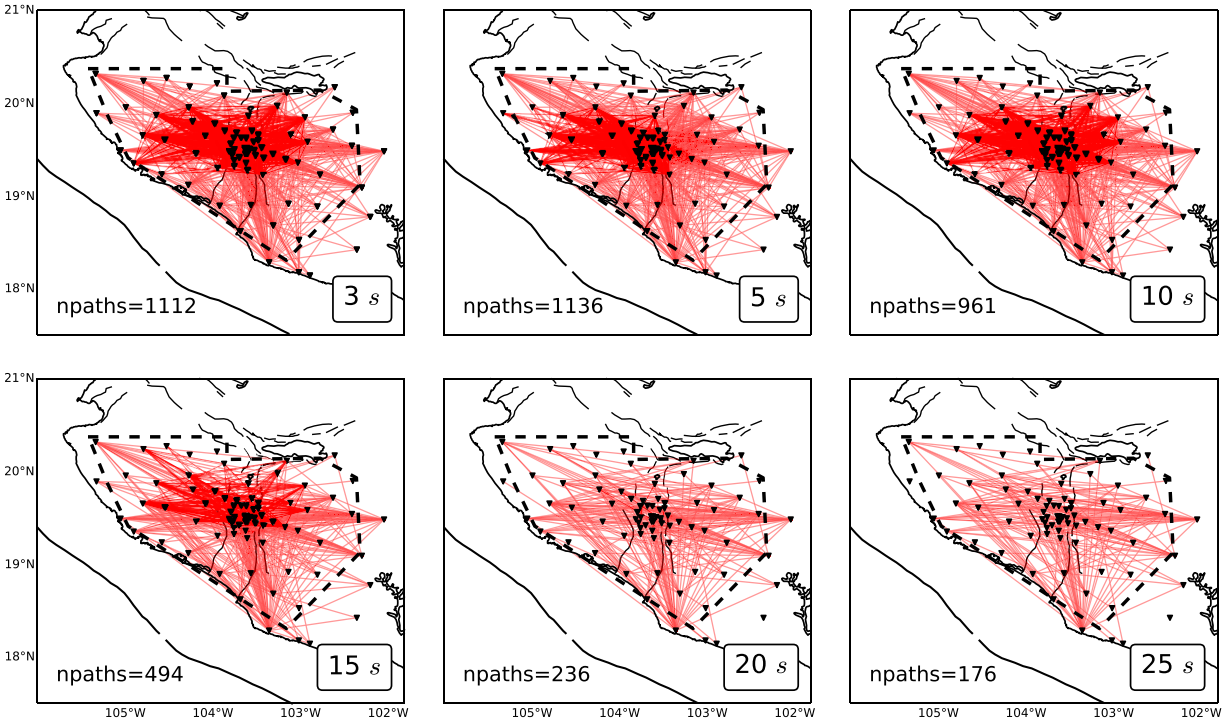

Fig. 5. Ray-path distribution for selected periods (5, 10, 15, 20 and 28 s). The number of rays used in the inversions is given at the bottom of each panel. The stations are depicted with black triangles. The black dashed polygon represents the satisfactory-resolution-box. Major tectonic features (black lines) are the same as in Fig. 1.

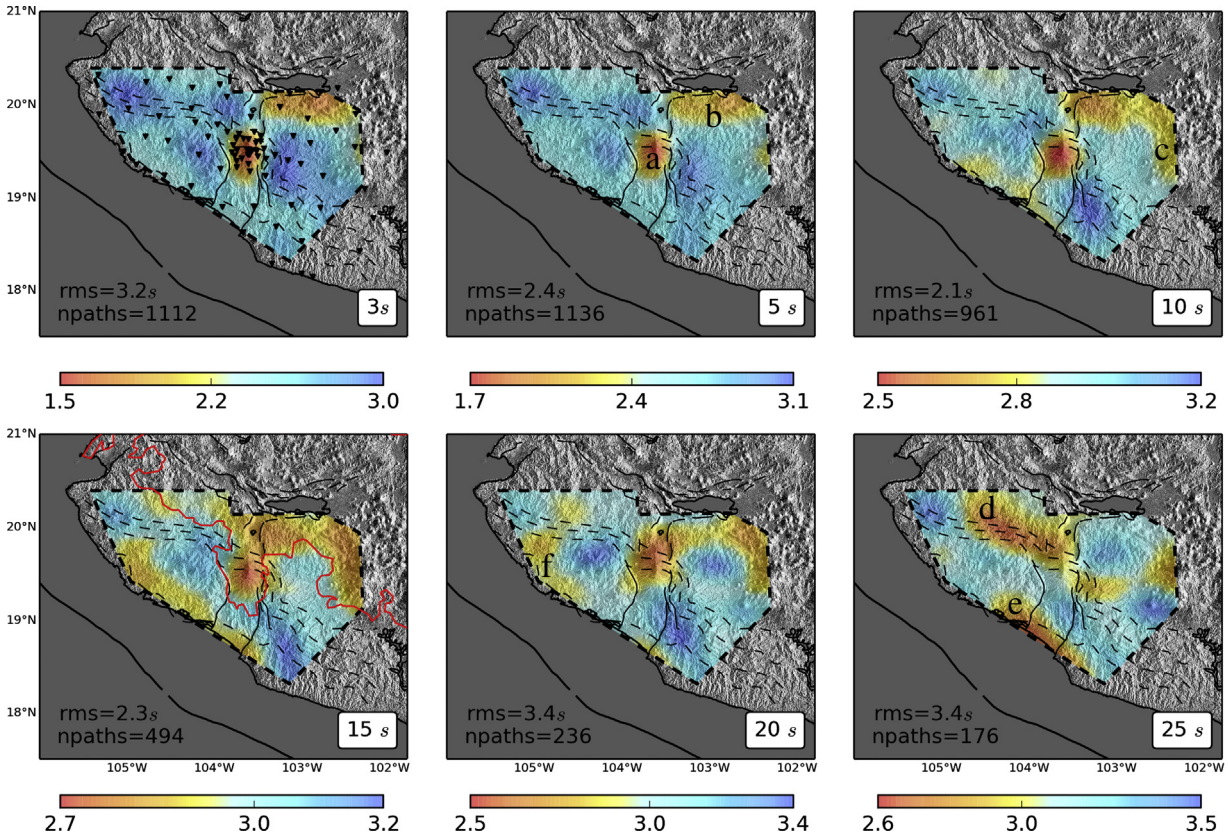

Fig. 6. Rayleigh-wave group velocity tomographic maps yielded by the inversions for selected periods of 3, 5, 10, 15, 20 and 25 s periods. Labels associated to velocity anomalies are referred in the text. The red outline in the 15 s map represents the southern limit of the TMVB. Major tectonic features (black lines) and subducting slab isodepth contours (dotted lines) are the same as in Fig. 1.

et al., 2008) and beneath the Toba caldera (Stankiewicz et al., 2010). Although numerous geophysical studies have been done in the CVC, no clear evidence of the Colima volcano magma chamber has ever been reported (e.g., Medina-Martínez et al., 1996; Zobin et al., 2002; López-Loera, 2012). This work confirms the presence of a magma chamber above ~7 km depth and provides insights of its horizontal geometry

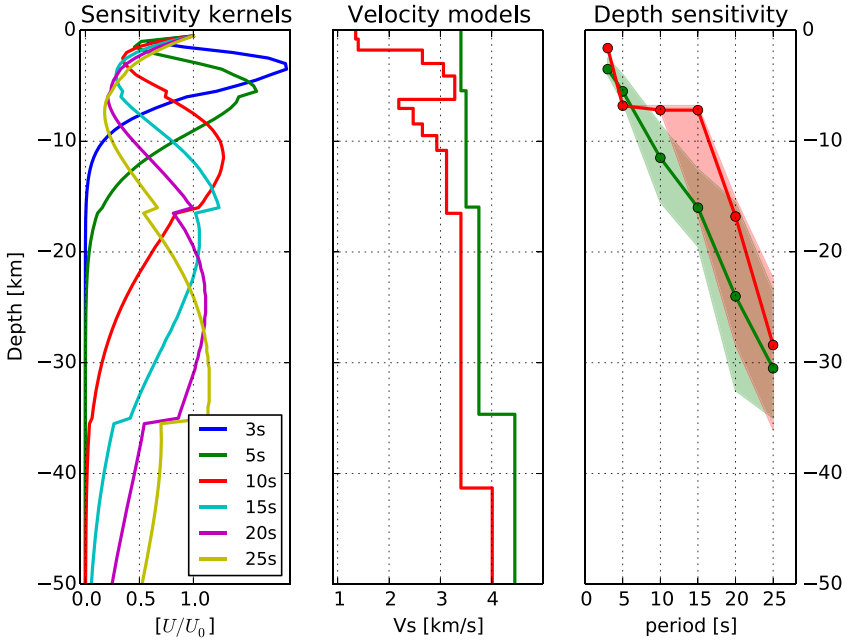

Fig. 7. Left: sensitivity kernels obtained for the velocity model by Iglesias et al. (2001); middle: velocity models (green: Iglesias et al. (2001); red: Cruz-Atienza et al. (2001)); right: maximum sensitivity depths (dots) for both models (same colors that middle panel) and associated ranges with 85% sensitivity (shaded zones).

(i.e., lengths of about 30 km in the east-west direction and about 50 km in the north-south graben axis), suggesting a structural control of the Colima graben fault system. Furthermore, although with higher group velocities (i.e., ~2.5 km/s), the CVC low-velocity body extends downward, rooting up to ~22 km depth (i.e., 20-s period) roughly below the volcano. This suggests the existence of a magma conduit allowing the molten material to rise from the deep crust and thus the existence of a magma reservoir at these depths, as proposed by Vigouroux et al. (2008). The existence of such conduit could be a consequence of the fracturing associated to the Colima graben, which facilitates the fluids rising from the subducted slab (e.g., Luhr, 1992).

4.2. The Michoacán-Guanajuato volcanic field

Another prominent east-west trending low-velocity feature appears to the south of the Chapala rift within the first ~7 km (i.e., for periods of 3 and 5 s). Such isolated body (denoted as "b" in the 5 s map of Fig. 6) then merges with a deeper system to the southeast (denoted as "c" in the 10 s map of Fig. 6) at depths larger than ~10 km, spreading all over the Michoacán-Guanajuato volcanic field (MGVF; i.e., beneath the Tancítaro volcano). Deeper, around 17–24 km depth (i.e., 15- and 20-s periods), the CVC and MGVF low-velocity bodies merge beneath the Colima rift, forming a horseshoe-like feature remarkably delineated by the southernmost edge of the TMVB (red line in the 15 s map of Fig. 6). The moderate group velocities of this large structure (around 2.7 km/s) and its spatial correlation with the monogenetic volcanism (gray dots in Fig. 1) indicate that the body may have a magmatic origin. Indeed, such a low-velocity zone may be the consequence of the slab dehydration, which promotes the accretion of deep magma bodies such as large batholiths. The connection between the CVC magmatic system and the MGVF low-velocity structure at ~22 km depth suggests either a deep source of magma mixing, as revealed by the anomalous enrichments of compatible trace elements in Colima andesites (e.g., Luhr and Carmichael, 1980), or the existence of a common magma source at that depth.

4.3. The Rivera plate mantle wedge

Deeper than ~30 km (i.e., 25 s), although a low-velocity root remains below the Tancítaro-Paricutín volcanoes, most of low-velocity features migrate to the northwest of the CVC describing an elongated slab-parallel body, right beneath the monogenetic Mascota, Ayutla and Tapalpa volcanic fields (MATVF; denoted as "d" in the 25 s map of Fig. 6). Considering both the Rivera slab geometry below the body, which abruptly increases its depth from ~40 to ~80 km (dashed lines in Fig. 6) (Suhardja, 2013; Abbott, 2014), and the thickness of the continental crust of ~35 km (Ferrari et al., 2011 and references therein; Suhardja, 2013), this low-velocity body may correspond to the mantle wedge above the Rivera plate. Indeed, the water release from the subducting slab serpentinizes the mantle wedge (e.g., Bostock et al., 2002), producing lower velocity anomalies as compared to the surrounding crustal minerals (Christensen, 1996). This phenomenon is accentuated by the steeper subduction angle of the Rivera plate, which induces a mantle wedge thickening away from the slab. Actually, by means of receiver function analysis, Suhardja (2013) inferred a serpentinized mantel wedge above the Rivera plate at distances of ~80 to ~100 km from the coast, which is consistent with our results (Fig. 6).

4.4. Volcanic deposits

The spatial correlation between the low-velocity bodies and the superficial volcanic activity is one of the most noticeable results of this study. The correlation is clear below (1) the Colima volcano in the center of the study area, (2) the Colima and south of the Chapala rifts to the north and northeast, (3) the MGVF to the east and (4) the MATVF to the northwest. Yet, depending on their locations, the correlation appears at different depths so that the shallower the low-velocity body, the younger are the associated volcanic deposits. For instance, in the currently active Colima volcano, we find the low-velocity anomaly above ~3 km depth (i.e., 3-s period). In the MGVF, where a low-velocity anomaly appears deeper, below ~10 km depth (i.e., 10-s period), the volcanism started in the late Pliocene (2.78 Ma; e.g., Gómez-Tuena et al., 2007) and the volume of material erupted in the last 40,000 years has been an order of magnitude less than the Colima stratovolcano (Ferrari et al., 2011). Moreover, in the MATVF, we find both the oldest lavas in the region with early Pliocene ages ranging from 4.5 to 4.69 Ma (e.g., Gómez-Tuena et al., 2007) and the deepest low-velocity body that probably reaches the mantle wedge, around 30 km depth (i.e., 25-s period). These observations strongly suggest that all mentioned low-velocity bodies have a magmatic origin and then may be responsible of the volcanisms in the entire region.

4.5. The subducting slab

An along-coast ~30 km width low-velocity zone appears around 28 km depth (i.e., 25-s period) primarily to the southeast of Manzanillo bay (denoted as "e" in the 25 s map of Fig. 6). Considering the geometry of the Cocos plate (Abbott, 2014), this body may correspond to the transition from continental to oceanic crusts. Although subducted basalts are generally observed in tomographic studies with higher velocities than the surrounding materials (e.g., Kárason and van der Hilst, 2000), recent studies concluded that the basalts may contain pervasive water and/or water-saturated oceanic sediments with low velocities at the very top of the slab (Audet et al., 2009). We thus interpret such low-velocity zone as the uppermost layer of the Cocos plate. This observation has also been done in the region by Suhardja (2013) and to the east, in the Guerrero segment of the Cocos plate (e.g., Pérez-Campos et al., 2008). Shallower, around 15 km depth (i.e., 15- and 20-s periods), the low-velocity zone appears to the northwest of the bay (denoted as "f" in the 20 s map of Fig. 6), possibly indicating the presence of the corresponding uppermost layer of the Rivera plate. These observations suggest that the Cocos plate subducts with a steeper angle than the Rivera plate beneath the first ~30 km from the coast (i.e., with a slope ~9° steeper if we assume a depth difference of 13 km between the plates at 80 km from the trench). This result is also in agreement with recent geophysical and geochemical studies (Andrews et al., 2011; Taran et al., 2013; Abbott, 2014) and joints both the idea of the slab tear between the subducting plates somewhere beneath Manzanillo bay and the hypothesis of the slab detachment in the region (e.g., Yang et al., 2009; Suhardja, 2013) that would allow the asthenosphere to rise above the plates to feed the Colima volcano.

Some of the interpretations of Sections 4.3, 4.4 and 4.5 are based on the 25 s tomographic map (Fig. 6). Even though the ray-path density at this period is the lowest (Fig. 5) and that smearing effects appeared in the associated checkerboard test (Fig. 4), we believe that our results are reliable enough to put forward the interpretations.

5. Conclusions

Detailed imaging of the crust was obtained across the Jalisco Block and western Michoacán from a Rayleigh-wave group velocity tomography by means of ambient noise cross correlations. Ambient noise tomography was performed using records of 78 seismic stations providing high-resolution images from ~2 to ~35 km depth. Results robustly show a deep and well-delineated volcanic system below the Colima volcano rooting up to ~22 km depth. Seismic evidence of low velocities in the upper 7 km indicates the presence of a shallow magmatic chamber associated to a larger geothermal system limited by the Colima graben fault system in the east-west direction. An independent east-west trending low-velocity zone to the south of the Chapala rift and west of the MGVF (i.e., beneath the Tancítaro-Paricutín volcanoes) spans up to ~15 km depth and then merges, underneath the Colima rift, with the

CVC low-velocity body at about 20 km depth. Such large horseshoe-shaped feature is perfectly delineated by the southernmost edge of the Trans-Mexican Volcanic Belt. For depths greater than ~30 km, low-velocity features become parallel to the slab strike, right beneath the MATFV to the northwest of the CVC, suggesting the presence of the serpentinized mantle wedge above the Rivera plate. Our results also show a spatial correlation between the low-velocity bodies in the region and the superficial volcanic activity. The correlation depends on both, the age of the associated deposits and the location of the bodies. We concluded that the age of volcanism along the Trans-Mexican Volcanic front in its western sector is directly correlated with depth of the low-velocity bodies, so that the shallower the bodies, the younger are the volcanic deposits. This strongly suggests that the low-velocity anomalies have a magmatic origin probably responsible of the overriding volcanism.

On the other hand, an along-coast ~30 km width low-velocity region to the southeast of the Manzanillo bay appears around 28 km depth. We interpret this region as the uppermost layer of the Cocos plate. Shallower, around 15 km depth, the low-velocity zone appears to the northwest of the bay, probably revealing the corresponding uppermost layer of the Rivera plate. These observations suggest that the Cocos plate subducts with an angle ~9° steeper than the Rivera plate and thus support the idea of the slab tear between both plates somewhere beneath Manzanillo, as suggested by previous works.

Acknowledgments

We thank Michel Campillo for clarifications on the sensitivity kernels, as well as Yuri Taran, Claus Siebe and Vladimir Kostoglodov for fruitful discussions. Instrumentation, field support and data access for the MARS and CODEX arrays was provided by the IRIS-PASSCAL Instrumentation Center. We also thank the staff from the 'Red Sismológica Telemétrica del Estado de Colima' (RESCO) and from the 'Servicio Sismológico Nacional' (SSN) to provide data access. This work was supported by the Consejo Nacional de Ciencia y Tecnología (CONACyT) through the graduate school scholarships and through projects numbers 129820 and #221165. We thank N. Rawlinson for making his tomography code available to us. The authors are grateful for thoughtful reviews by Philippe Jousset and an anonymous referee.

References

Abbott, E.R., 2014. Shallow seismicity patterns in the northwestern section of the Mexico subduction zone. (M.S. Thesis) Miami University, Miami, Florida.
Aki, K., Richards, P., 2002. Quantitative seismology. University Science Book.
Andrews, V., Stock, J., Vázquez, C.A.R., Reyes-Dávila, G., 2011. Double-difference relocation of the aftershocks of the Tecomán, Colima, Mexico Earthquake of 22 January 2003. Pure Appl. Geophys. 168, 1331–1338. http://dx.doi.org/10.1007/s00024-010-0203-0.
Audet, P., Bostock, M.G., Christensen, N.I., Peacock, S.M., 2009. Seismic evidence for overpressured subducted oceanic crust and megathrust fault sealing. Nature 457, 76–78. http://dx.doi.org/10.1038/nature07650.
Bandy, W.L., Hilde, T.W.C., Yan, C.Y., 2000. The Rivera-Cocos plate boundary: implications for Rivera-Cocos relative motion and plate fragmentation. Geol. Soc. Am. Spec. Pap. 334, 1–28. http://dx.doi.org/10.1130/0-8137-2334-5.1.
Bensen, G.D., Ritzwoller, M.H., Barmin, M.P., Levshin, A.L., Lin, F., Moschetti, M.P., Shapiro, N.M., Yang, Y., 2007. Processing seismic ambient noise data to obtain reliable broad-band surface wave dispersion measurements. Geophys. J. Int. 169, 1239–1260. http://dx.doi.org/10.1111/j.1365-246X.2007.03374.x.
Bostock, M.G., Hyndman, R.D., Rondenay, S., Peacock, S.M., 2002. An inverted continental Moho and serpentinization of the forearc mantle. Nature 417, 536–538. http://dx.doi.org/10.1038/417536a.
Brenguier, F., Shapiro, N.M., Campillo, M., Nercessian, A., Ferrazzini, V., 2007. 3-D surface wave tomography of the Piton de la Fournaise volcano using seismic noise correlations. Geophys. Res. Lett. 34 (2). http://dx.doi.org/10.1029/2006GL028586.
Christensen, N.I., 1996. Poisson's ratio and crustal seismology. J. Geophys. Res. 101, 3139–3156. http://dx.doi.org/10.1029/95JB03446.
Cruz-Atienza, V.M., Pacheco, J.F., Singh, S.K., Shapiro, N.M., Valdés, C., Iglesias, A., 2001. Size of Popocatepetl Volcano explosions (1997–2001) from waveform inversion. Geophys. Res. Lett. 28, 4027–4030. http://dx.doi.org/10.1029/2001GL013207.
de Kool, M., Rawlinson, N., Sambridge, M., 2006. A practical grid-based method for tracking multiple refraction and reflection phases in three-dimensional heterogeneous media. Geophys. J. Int. 167, 253–270. http://dx.doi.org/10.1111/j.1365-246X.2006.03078.x.
DeMets, C., Traylen, S., 2000. Motion of the Rivera plate since 10 Ma relative to the Pacific and North American plates and the mantle. Tectonophysics 318, 119–159. http://dx.doi.org/10.1016/S0040-1951(99)00309-1.
Dougherty, S.L., Clayton, R.W., Helmberger, D.V., 2012. Seismic structure in central Mexico: implications for fragmentation of the subducted Cocos plate. J. Geophys. Res. Solid Earth 117, 9316. http://dx.doi.org/10.1029/2012JB009528.
Dziewonski, A., Bloch, S., Landisman, M., 1969. A technique for the analysis of transient seismic signals. Bull. Seismol. Soc. Am. 59, 427–444.
Ferrari, L., Rosas-Elguera, J., 2000. Late Miocene to Quaternary extension at the northern boundary of the Jalisco Block, western Mexico: the Tepic-Zacoalco Rift revised. Geol. Soc. Am. Spec. Pap. 334, 41–63. http://dx.doi.org/10.1130/0-8137-2334-5.41.
Ferrari, L., Pasquaré, G., Venegas-Salgado, S., Romero-Rios, F., 2000. Geology of the western Mexican Volcanic Belt and adjacent Sierra Madre Occidental and Jalisco Block. Geol. Soc. Am. Spec. Pap. 334, 65–83. http://dx.doi.org/10.1130/0-8137-2334-5.65.
Ferrari, L., Petrone, C.M., Francalanci, L., 2001. Generation of oceanic-island basalt–type volcanism in the western Trans-Mexican volcanic belt by slab rollback, asthenosphere infiltration, and variable flux melting. Geology 29, 507–510. http://dx.doi.org/10.1130/0091-7613(2001)029<0507:GOOIBT>2.0.CO;2.
Ferrari, L., Orozco-Esquivel, T., Manea, V., Manea, M., 2011. The dynamic history of the Trans-Mexican Volcanic Belt and the Mexico subduction zone. Tectonophysics 522–523, 122–149. http://dx.doi.org/10.1016/j.tecto.2011.09.018.
Frey, H.M., Lange, R.A., Hall, C.M., Delgado-Granados, H., Carmichael, I.S.E., 2007. A Pliocene ignimbrite flare-up along the Tepic-Zacoalco rift: evidence for the initial stages of rifting between the Jalisco block (Mexico) and North America. Geol. Soc. Am. Bull. 119, 49–64. http://dx.doi.org/10.1130/B25950.1.
Gaviria, P., Ramón, J., Gutiérrez, M.A.C., Bandy, W.L., Michaud, F., 2013. Morphology and magnetic survey of the Rivera-Cocos plate boundary of Colima, Mexico. Geofis. Int. 52, 73–85.
Gómez-Tuena, A., Orozco-Esquivel, M.T., Ferrari, L., 2007. Igneous petrogenesis of the Trans-Mexican Volcanic Belt. Geol. Soc. Am. Spec. Pap. 422, 129–181. http://dx.doi.org/10.1130/2007.2422(05).
Herrmann, R.B., 1989. Computer Programs in Seismology. University.
Iglesias, A., Cruz-Atienza, V.M., Shapiro, N.M., Singh, S.K., Pacheco, J.F., 2001. Crustal structure of south-central Mexico estimated from the inversion of surface-wave dispersion curves using genetic and simulated annealing algorithms. Geofis. Int. 40 (3), 181–190.
Kárason, H., Van Der Hilst, R.D., 2000. Constraints on mantle convection from seismic tomography. Hist. Dyn. Glob. Plate Motions 277–288 http://dx.doi.org/10.1029/GM121p0277.
Kostoglodov, V., Bandy, W.L., 1995. Seismotectonic constraints on the convergence rate between the Rivera and North American plates. J. Geophys. Res. 100, 17977–17989. http://dx.doi.org/10.1029/95JB01484.
Lees, J.M., 2007. Seismic tomography of magmatic systems. J. Volcanol. Geotherm. Res. Large Silicic Magma Syst. 167, 37–56. http://dx.doi.org/10.1016/j.jvolgeores.2007.06.008.
Lévêque, J.-J., Rivera, L., Wittlinger, G., 1993. On the use of the checker-board test to assess the resolution of tomographic inversions. Geophys. J. Int. 115, 313–318. http://dx.doi.org/10.1111/j.1365-246X.1993.tb05605.x.
Levshin, A.L., 1989. Seismic Surface Waves in a Laterally Inhomogeneous Earth.
López-Loera, H., 2012. 2 ¾ dimension modeling of the aeromagnetic anomaly of Volcán de Colima, western Mexico. Geofis. Int. 51, 129–142.
Luhr, J.F., 1992. Slab-derived fluids and partial melting in subduction zones: insights from two contrasting Mexican volcanoes (Colima and Ceboruco). J. Volcanol. Geotherm. Res. 54, 1–18. http://dx.doi.org/10.1016/0377-0273(92)90111-P.
Luhr, J.F., Carmichael, I.S.E., 1980. The Colima volcanic complex, Mexico. Contrib. Mineral. Petrol. 71 (4), 343–372. http://dx.doi.org/10.1007/BF00374707.
Manea, V., Manea, M., Kostoglodov, V., Sewell, G., 2006. Intraslab seismicity and termal stress in the subducted Cocos plate beneath central Mexico. Tectonophysics 420, 389–408. http://dx.doi.org/10.1016/j.tecto.2006.03.029.
Medina-Martínez, F., Espíndola, J.M., De la Fuente, M., Mena, M., 1996. A gravity model of the Colima. Geofis. Int. 35 (4), 409-114.
Menke, W., 2012. Geophysical Data Analysis: Discrete Inverse Theory. Academic Press.
Mordret, A., Landès, M., Shapiro, N.M., Singh, S.C., Roux, P., Barkved, O.I., 2013. Near-surface study at the Valhall oil field from ambient noise surface wave tomography. Geophys. J. Int. 193, 1627–1643. http://dx.doi.org/10.1093/gji/ggt061.
Pardo, M., Suárez, G., 1995. Shape of the subducted Rivera and Cocos plates in southern Mexico: seismic and tectonic implications. J. Geophys. Res. 100, 12357–12373. http://dx.doi.org/10.1029/95JB00919.
Pérez-Campos, X., Kim, Y., Husker, A., Davis, P.M., Clayton, R.W., Iglesias, A., Pacheco, J.F., Singh, S.K., Manea, V.C., Gurnis, M., 2008. Horizontal subduction and truncation of the Cocos Plate beneath central Mexico. Geophys. Res. Lett. 35, L18303. http://dx.doi.org/10.1029/2008GL035127.
Rawlinson, N., Sambridge, M., 2004. Wave front evolution in strongly heterogeneous layered media using the fast marching method. Geophys. J. Int. 156, 631–647. http://dx.doi.org/10.1111/j.1365-246X.2004.02153.x.
Rawlinson, N., Hauser, J., Sambridge, M., 2008. Seismic ray tracing and wavefront tracking in laterally heterogeneous media. Adv. Geophys. 49, 203.
Rosas-Elguera, J., Ferrari, L., Garduno-Monroy, V.H., Urrutia-Fucugauchi, J., 1996. Continental boundaries of the Jalisco Block and their influence in Pliocene–Quaternary kinematics of western Mexico. Geology 24, 921–924. http://dx.doi.org/10.1130/0091-7613(1996)024<0921:CBOTJB>2.3.CO;2.
Sabra, K.G., Gerstoft, P., Roux, P., Kuperman, W.A., Fehler, M.C., 2005. Extracting time-domain Green's function estimates from ambient seismic noise. Geophys. Res. Lett. 32, L03310. http://dx.doi.org/10.1029/2004GL021862.
Sánchez-Sesma, F.J., Campillo, M., 2006. Retrieval of the Green's function from cross correlation: the canonical elastic problem. Bull. Seismol. Soc. Am. 96, 1182–1191. http://dx.doi.org/10.1785/0120050181.
Saygin, E., Kennett, B.L.N., 2010. Ambient seismic noise tomography of Australian continent. Tectonophysics 481, 116–125. http://dx.doi.org/10.1016/j.tecto.2008.11.013.

Schaaf, P., Moran-Zenteno, D., Hernandez-Bernal, M.S., Solis-Pichardo, G., Tolson, G., Kohler, H., 1995. Paleogene continental margin truncation in southwestern Mexico: geochronological evidence. Tectonics 14, 1339–1350. http://dx.doi.org/10.1029/95TC01928.

Serrato-Díaz, G.S., Bandy, W.L., Gutiérrez, C.A.M., 2004. Active rifting and crustal thinning along the Rivera-Cocos plate boundary as inferred from Mantle Bouguer gravity anomalies. Geofis. Int. 43 (3), 361.

Sethian, J.A., 1996. A fast marching level set method for monotonically advancing fronts. Proc. Natl. Acad. Sci. 93, 1591–1595.

Shapiro, N.M., Campillo, M., 2004. Emergence of broadband Rayleigh waves from correlations of the ambient seismic noise. Geophys. Res. Lett. 31 (7). http://dx.doi.org/10.1029/2004GL019491.

Shapiro, N.M., Singh, S.K., 1999. A systematic error in estimating surface-wave group-velocity dispersion curves and a procedure for its correction. Bull. Seismol. Soc. Am. 89, 1138–1142.

Shapiro, N.M., Campillo, M., Stehly, L., Ritzwoller, M.H., 2005. High-resolution surface-wave tomography from ambient seismic noise. Science 307, 1615–1618. http://dx.doi.org/10.1126/science.1108339.

Shen, Y., Ren, Y., Gao, H., Savage, B., 2012. An Improved method to extract very broadband empirical green's functions from ambient seismic noise. Bull. Seismol. Soc. Am. 102 (4), 1872–1877. http://dx.doi.org/10.1785/0120120023.

Skinner, S.M., Clayton, R.W., 2011. An evaluation of proposed mechanism of slab flattening in Central Mexico. Pure Appl. Geophys. 168, 1461–1474. http://dx.doi.org/10.1007/s00024-010-0200-3.

Soto, G.L., Ni, J.F., Grand, S.P., Sandvol, E., Valenzuela, R.W., Speziale, M.G., González, J.M.G., Reyes, T.D., 2009. Mantle flow in the Rivera–Cocos subduction zone. Geophys. J. Int. 179, 1004–1012. http://dx.doi.org/10.1111/j.1365-246X.2009.04352.x.

Stachnik, J.C., Dueker, K., Schutt, D.L., Yuan, H., 2008. Imaging Yellowstone plume-lithosphere interactions from inversion of ballistic and diffusive Rayleigh wave dispersion and crustal thickness data. Geochem. Geophys. Geosyst. 9 (6), Q06004. http://dx.doi.org/10.1029/2008GC001992.

Stankiewicz, J., Ryberg, T., Haberland, C., Fauzi Natawidjaja, D., 2010. Lake Toba volcano magma chamber imaged by ambient seismic noise tomography. Geophys. Res. Lett. 37 (17). http://dx.doi.org/10.1029/2010GL044211.

Stehly, L., Fry, B., Campillo, M., Shapiro, N.M., Guilbert, J., Boschi, L., Giardini, D., 2009. Tomography of the Alpine region from observations of seismic ambient noise. Geophys. J. Int. 178, 338–350. http://dx.doi.org/10.1111/j.1365-246X.2009.04132.x.

Suhardja, S.K., 2013. Mapping the Rivera and Cocos Subduction Zone. (Ph.D. Thesis) University of Texas, Austin.

Taran, Y., Morán-Zenteno, D., Inguaggiato, S., Varley, N., Luna-González, L., 2013. Geochemistry of thermal springs and geodynamics of the convergent Mexican Pacific margin. Chem. Geol. Front. Gas Geochem. 339, 251–262. http://dx.doi.org/10.1016/j.chemgeo.2012.08.025.

Vigouroux, N., Wallace, P.J., Kent, A.J.R., 2008. Volatiles in high-K magmas from the western trans-Mexican volcanic belt: evidence for fluid fluxing and extreme enrichment of the mantle wedge by subduction processes. J. Petrol. 49, 1589–1618. http://dx.doi.org/10.1093/petrology/egn039.

Weaver, R.L., 2005. Information from seismic noise. Science 307, 1568–1569. http://dx.doi.org/10.1126/science.1109834.

Yang, T., Grand, S.P., Wilson, D., Guzman-Speziale, M., Gomez-Gonzalez, J.M., Dominguez-Reyes, T., Ni, J., 2009. Seismic structure beneath the Rivera subduction zone from finite-frequency seismic tomography. J. Geophys. Res. 114, B01302. http://dx.doi.org/10.1029/2008JB005830.

Zobin, V.M., Luhr, J.F., Taran, Y.A., Bretón, M., Cortés, A., de La Cruz-Reyna, S., Domínguez, T., Galindo, I., Gavilanes, J.C., Muñiz, J.J., Navarro, C., Ramírez, J.J., Reyes, G.A., Ursúa, M., Velasco, J., Alatorre, E., Santiago, H., 2002. Overview of the 1997–2000 activity of Volcán de Colima, México. J. Volcanol. Geotherm. Res. 117, 1–19. http://dx.doi.org/10.1016/S0377-0273(02)00232-9.